

## High-Pressure Vibrational Spectroscopy of Energetic Materials: Hexahydro-1,3,5-trinitro-1,3,5-triazine

Jennifer A. Ciezak,<sup>\*,†,‡</sup> Timothy A. Jenkins,<sup>‡</sup> Zhenxian Liu,<sup>‡</sup> and Russell J. Hemley<sup>‡</sup>

BWCD-PSB-WMRD, U.S. Army Research Laboratory, Aberdeen Proving Ground, Maryland 21005, and Geophysical Laboratory, Carnegie Institution of Washington, 5251 Broad Branch Road NW, Washington, D.C. 20015-1305

Received: May 23, 2006; In Final Form: October 18, 2006

Vibrational spectroscopy has been used to investigate the room-temperature high-pressure phases of the energetic material hexahydro-1,3,5-trinitro-1,3,5-triazine (RDX). The pressure-induced alterations in the spectral profiles were studied in a compression sequence to 30.2 GPa using Raman spectroscopy and to 26.6 GPa using far-infrared spectroscopy. At pressures near 4.0 GPa, several changes become immediately apparent in the Raman spectrum, such as large frequency shifts, mode splittings, and intensity changes, which are associated with a phase transition from  $\alpha$ -RDX to  $\gamma$ -RDX. Our study extends the kinetic stability of  $\gamma$ -RDX to pressures near 18.0 GPa. Evidence for a new phase was found at pressures between 17.8 and 18.8 GPa and is based on the appearance of new vibrational bands and associated changes in intensity patterns. The new phase has vibrational characteristics that are similar to those of  $\beta$ -RDX, suggesting the two polymorphs share a related crystal structure.

### Introduction

Hexahydro-1,3,5-trinitro-1,3,5-triazine (RDX) is one of the most widely employed high explosives in military applications today. The extensive use of RDX stems from its reasonable insensitivity to external conditions, high performance level, and relatively easy and inexpensive synthesis. In the past 30 years, RDX has been the subject of numerous experimental and theoretical reports aimed at understanding the structural,<sup>1–4</sup> electronic,<sup>5–9</sup> mechanical,<sup>10</sup> thermal expansion,<sup>11–13</sup> vibrational,<sup>14–18</sup> and elastic<sup>19</sup> properties and, more recently, toxicological effects.<sup>20</sup> However, its widespread use in many explosive formulations dictates a need to understand the material properties, not only at ambient conditions, but also under extreme conditions within high-pressure/high-temperature regimes that can lead to shock-initiated detonation.

The fundamental physical characteristics of the room-temperature, ambient-pressure form of RDX ( $\alpha$ -RDX), shown in Figure 1, have been elucidated by X-ray<sup>1–3</sup> and neutron<sup>4</sup> diffraction.  $\alpha$ -RDX has an orthorhombic structure with eight molecules per unit cell, a space group of *Pbca*, and cell parameters of  $a = 13.182(2)$  Å,  $b = 11.574(2)$  Å, and  $c = 10.709(2)$  Å. Within the crystalline environment, the nitro groups of each RDX molecule are pseudoplanar and are arranged in a chair conformation, with two of the three groups in the axial position with respect to the *s*-triazine ring.<sup>4</sup> The RDX site symmetry within the crystallographic cell is  $C_1$ , but each molecule possesses a near plane of symmetry defined by one of the methylene groups and the N–N bond on the opposite end of the molecule. Numerous spectral features associated with the internal and lattice vibrational modes of  $\alpha$ -RDX have been observed and assigned,<sup>14–18</sup> and recently, the symmetries of all 24 Raman-active optical phonons were identified.<sup>15</sup>

In contrast to the extensive experimental data available for  $\alpha$ -RDX, there has been limited experimental characterization of the high-pressure/temperature phases of RDX. High-pressure vibrational spectroscopy<sup>21</sup> and X-ray diffraction<sup>22</sup> of RDX were performed nearly two decades ago, but only to pressures of 12.2 and 9.2 GPa, respectively. Within this narrow pressure range, evidence was found for an additional room-temperature phase,  $\gamma$ -RDX. The crystalline structure of  $\gamma$ -RDX has yet to be fully resolved, but preliminary evidence has alluded to an orthorhombic crystal symmetry, similar to that of  $\alpha$ -RDX, with eight molecules per unit cell.<sup>22</sup> A high-temperature phase,  $\beta$ -RDX, has been reported as an extremely short-lived room-temperature polymorph which results from rapid crystallization of RDX from boiling solvents.<sup>16,21</sup>  $\beta$ -RDX is also the predominant phase in solutions. Although spectroscopic analysis of  $\beta$ -RDX supports a molecular structure similar to that of  $\alpha$ -RDX,<sup>16</sup> the vibrational pattern of  $\beta$ -RDX shows several vibrational modes present in the  $\alpha$ -RDX phase collapse into single, doubly degenerate vibrations, possibly because of higher molecular symmetry. Further vibrational analysis has suggested that  $\beta$ -RDX has essentially  $C_{3v}$  symmetry, but the results could not provide a more detailed description of the molecular structure.<sup>16,21</sup>

The results presented here expand in depth on previously reported material<sup>14–18,21,22</sup> and are part of a research program aimed at extending the current understanding of pressure-driven structural transformations of energetic materials through employment of a multitechnique approach. We performed in situ room-temperature, high-pressure Raman scattering studies of RDX in a compression sequence from ambient pressure to 30.2 GPa, as well as synchrotron infrared measurements from ambient pressure to 26.6 GPa. The primary goal of this study was to follow possible pressure-induced structural transformations in RDX at room temperature.

<sup>†</sup> U.S. Army Research Laboratory.

<sup>‡</sup> Carnegie Institution of Washington.

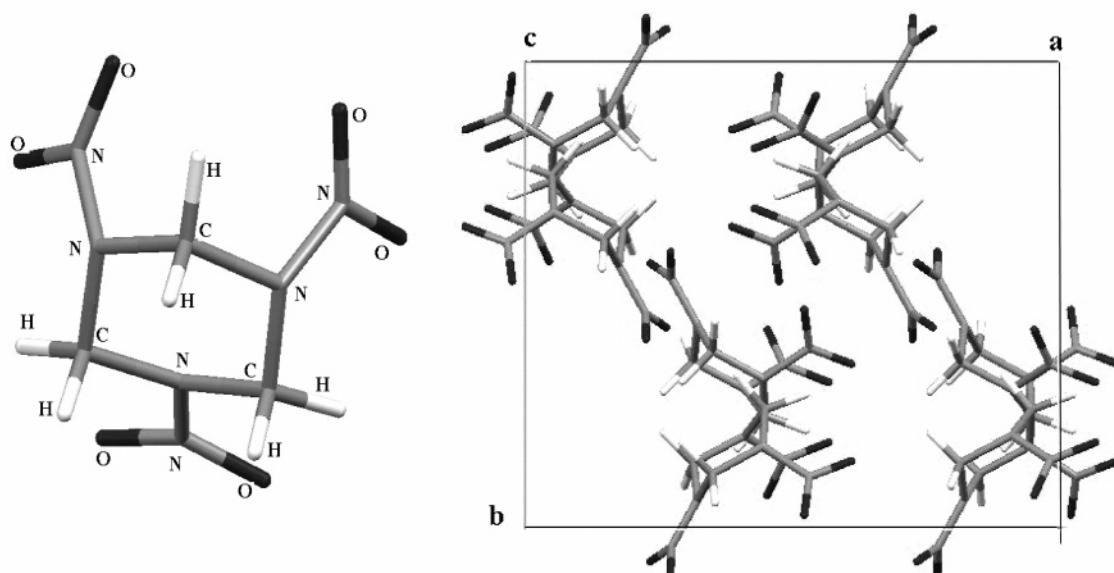


**Figure 1.** (Left) molecular structure of RDX. (Right) unit cell of RDX molecules.

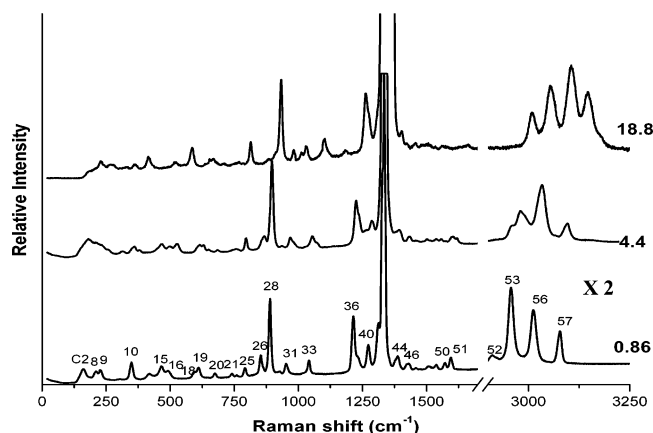


**Figure 2.** Selected high-pressure Raman spectra of RDX collected from 0.86 to 30.2 GPa at room temperature. The spectrum shown at 0.86 GPa is shown to scale between 0 and 1750  $\text{cm}^{-1}$ ; the spectra shown at 4.4 and 18.8 GPa are offset for clarity. The spectra are scaled by 2 between 2900 and 3250  $\text{cm}^{-1}$  for pressures between 0.86 and 18.8 GPa. The spectral region between 1700 and 2900  $\text{cm}^{-1}$  is omitted because of the low spectral intensity of the vibrational modes within this energy range. The vibrational modes are numbered according to ref 14 and Table 1.

### Experimental Details

Polycrystalline RDX was obtained from the Naval Surface Warfare Center at Indian Head, MD, and recrystallized in acetone to remove impurities. Piston-cylinder-type diamond anvil cells (DACs) were used for all experiments. The RDX sample was lightly ground into a fine powder and placed in a sample well preindented into a rhenium gasket with an approximately 120  $\mu\text{m}$  diameter and a depth of 35  $\mu\text{m}$ . The pressure was determined from the shift of the  $R_1$  ruby fluorescence line with pressure, which is precise to  $\pm 0.05$  GPa under quasi-hydrostatic conditions.<sup>23</sup> Helium was gas-loaded into the DAC for the Raman experiments using a method previously described.<sup>24</sup> White petroleum jelly was used as the pressure medium during the infrared experiments.

High-pressure Raman experiments were performed using the 488.0 nm line of an argon ion laser (Coherent Innova 90) as

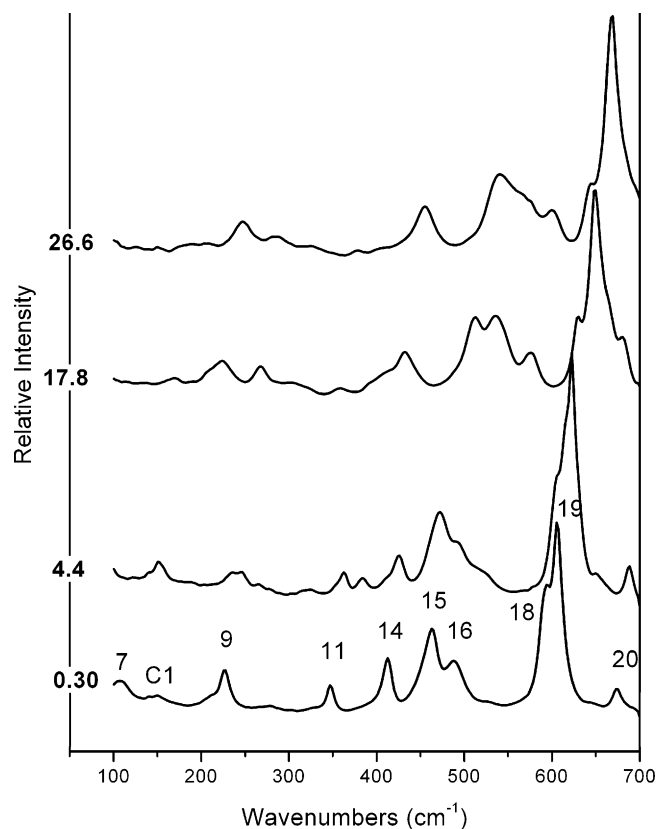


**Figure 3.** Selected high-pressure infrared spectra obtained in a compression sequence from 0.30 to 26.6 GPa. The spectrum presented at 0.30 GPa is to scale, while the remaining spectra are scaled and offset for clarity. The vibrational modes are numbered according to ref 14 and Table 1.

the excitation source, with output power kept at less than 0.1 W. A 460 mm focal length  $f/5.3$  imaging spectrograph (ISA HR 460) equipped with an 1800 grooves/mm grating with a resolution of  $\pm 0.5$   $\text{cm}^{-1}$  was used. The wavelength calibration was performed using a neon light and has an accuracy of  $\pm 1$   $\text{cm}^{-1}$ .

Synchrotron IR-absorption experiments were performed at beamline U2A of the National Synchrotron Light Source (NSLS)

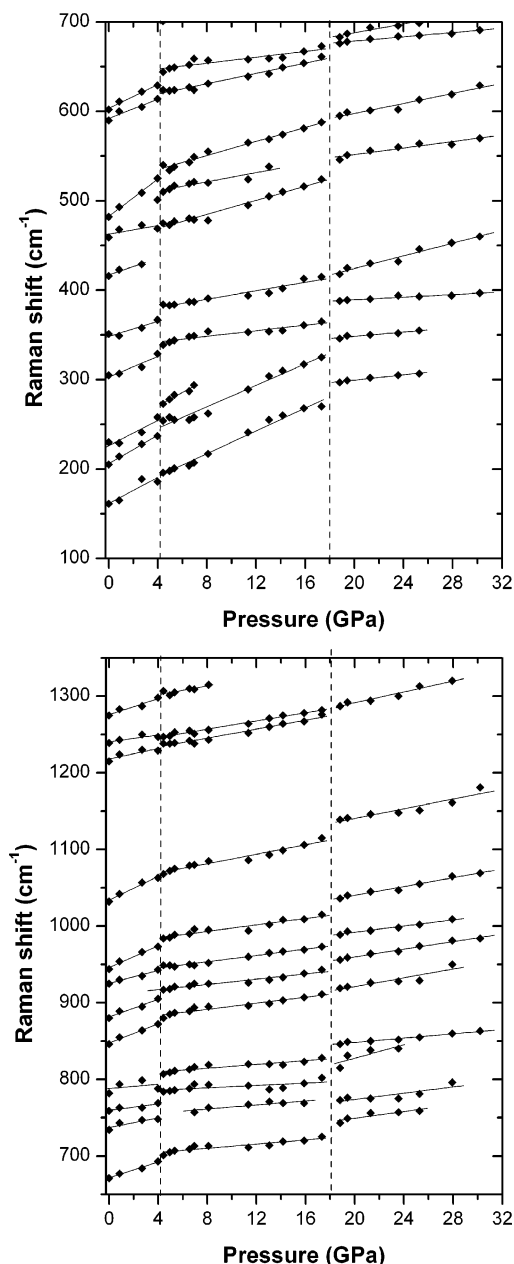


**Figure 4.** Pressure-induced Raman peak shifts of RDX. Previous studies have identified a phase transition near 4 GPa. The abrupt slope changes in the frequency shifts also indicate the onset of a phase transition near 18 GPa. Dashed lines indicate apparent phase boundaries. Linear fits are shown for the frequency shifts.

of Brookhaven National Laboratory (BNL). The synchrotron light is extracted from the VUV storage ring in a  $40 \times 40$  mrad solid angle. The collimated beam is delivered through a vacuum pipe system and directed into a Bruker IFS 66v Fourier transform infrared (FTIR) spectrometer. Extensive detail of the optical layout of this beamline is available.<sup>25</sup> The resolution used for all measurements was  $4 \text{ cm}^{-1}$ .

## Results and Discussion

Several representative Raman and infrared spectra of polycrystalline RDX on isothermal compression at 298 K to 30.2 GPa are shown in Figures 2 and 3, respectively. The frequencies of the vibrational bands are plotted as a function of pressure in Figures 4 and 5. The 36 fundamental Raman-active vibrations were identified by Haycraft et al.<sup>15</sup> using single-crystal polarized Raman scattering. The present data include the majority of these

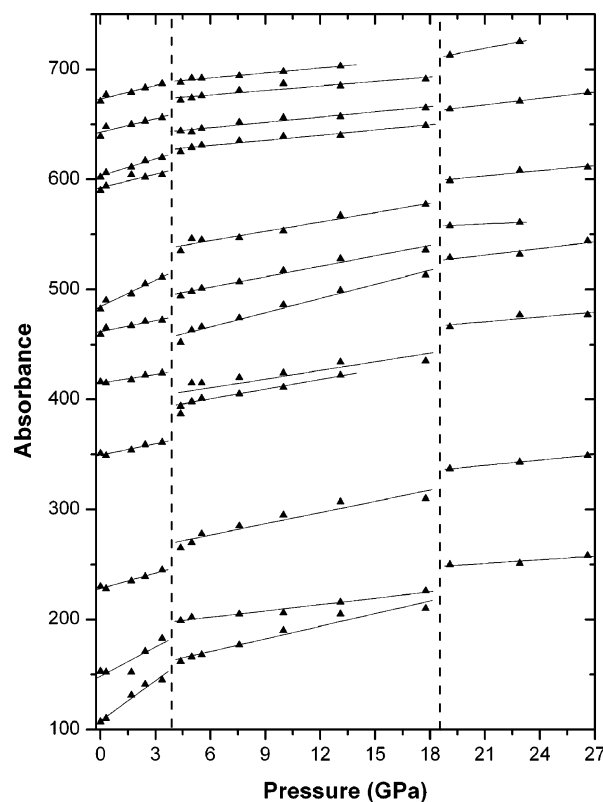


**Figure 5.** Pressure dependence of the frequencies of the IR-active modes. Dashed lines indicate apparent phase boundaries. Linear fits are shown for the frequency shifts.

peaks, which are utilized in the interpretation of the high-pressure behavior.

At pressures of and lower than 4.0 GPa, all vibrational modes display nearly linear shifts in frequency with pressure. Previous high-pressure spectroscopy<sup>21</sup> and X-ray diffraction<sup>22</sup> have demonstrated that a reversible phase transition to  $\gamma$ -RDX occurs at room temperature near 4.0 GPa. This transition is manifested in the spectroscopic data by changes in the pressure shifts of the infrared and Raman mode frequencies ( $dv/dP$ ), shown in Table 1, and on the basis of the available data has been interpreted to not produce significant changes in the crystalline framework.<sup>22</sup> The  $\gamma$ -RDX phase remains kinetically stable until somewhere between 17.8 and 18.8 GPa, where prominent discontinuities in the frequency shifts suggest the existence of another phase transition. This higher pressure transition was not identified in the previous work. On the basis of the large frequency shifts, it seems likely that this new phase, which we are terming  $\delta$ , is accompanied by structural changes within the crystalline framework.

One of the primary motivations for the current spectroscopic measurements was to determine the spectroscopic signatures of  $\gamma$ -RDX and  $\delta$ -RDX. In both the infrared and Raman measurements, we observe changes in many of the band shifts near the pressure of the phase transition. The  $\alpha \rightarrow \gamma$  transition near 4.0 GPa is coincident with a splitting of the  $353 \text{ cm}^{-1}$  ring twisting band, and the  $856 \text{ cm}^{-1}$  C–N stretching vibration begins to inhomogeneously broaden after the transition. However, the most obvious change in the Raman spectrum is observed in the C–H stretching region where a large intensity decrease of the  $2949 \text{ cm}^{-1}$  axial stretching mode is accompanied by the formation of a lower energy shoulder. This shoulder results from the large frequency shift of the  $2911 \text{ cm}^{-1}$  axial stretching mode. Examination of the infrared spectra above 4.0 GPa reveals vibrational trends that are similar to the Raman

**TABLE 1: Raman and Infrared Frequency Shifts of the Observed RDX Vibrational Bands up to 30.2 and 26.6 GPa, Respectively<sup>a</sup>**

(dν/dP) <sub>0</sub> , Raman	this work		reference			mode identification <sup>d</sup>	molecular motion	
	(dν/dP) <sub>0</sub> , infrared	γ, Raman	γ, infrared	Raman <sup>b</sup>	IR <sup>b,c</sup>			INS <sup>d</sup>
	12.2 (±1.2)		1.7	106	104	107	7	molecular bend + NO <sub>2</sub> rotation
	10.8 (±1.0)		1.1			153	C1	combination band, NO <sub>2</sub> torsional modes
7.5 (±0.5)		0.6				161	C2	combination band, NO <sub>2</sub> torsional modes
8.8 (±0.5)		0.6		205	208	205	8	N–NC <sub>2</sub> umbrella (eq) + NO <sub>2</sub> rotation (ax)
7.1 (±0.5)	7.1 (±0.5)	0.7	0.4	224	223	230	9	ring rotation + NO <sub>2</sub> rotation (all)
3.3 (±0.3)		0.4				305	10	molecular stretch
4.0 (±0.3)	4.1 (±0.4)	0.3	0.2	347	345	351	11	ring twist
5.5 (±0.4)	5.6 (±0.5)		0.1	414	410	416	14	ring bending (folding)
1.5 (±0.2)	1.5 (±0.2)	0.1	0.1	463	461	459	15	ring bending (folding) + N–N stretch (ax)
8.0 (±0.5)	7.7 (±0.6)	0.4	0.2	486	486	482	16	ring twist + NO <sub>2</sub> rock (eq)
6.8 (±0.4)	6.5 (±0.5)	0.2	0.1	588	589	590	18	ring bend
5.5 (±0.4)	5.4 (±0.4)	0.2	0.1	605	602	602	19	ring rock
4.3 (±0.4)	4.4 (±0.3)	0.1	0.1	669	670	671	20	ring bend
0.5 (±0.1)		0.1		739	738 (739)	734	21	N–NO <sub>2</sub> umbrella (ax)
3.0 (±0.2)		0.1		786	783 (782)	782	25	C–N stretch + NO <sub>2</sub> scissors (eq)
4.3 (±0.3)		0.1		847	844 (844)	843	26	N–N stretch + NO <sub>2</sub> scissors (ax)
3.5 (±0.2)		0.1		884	883 (883)	880	28	C–N stretch + CH <sub>2</sub> rock + N–N stretch
6.3 (±0.4)		0.1		943	947 (947)	944	31	N–N stretch (eq) + CH <sub>2</sub> twist + CH <sub>2</sub> rock
6.0 (±0.4)		0.1		1029	1040 (1039)	1032	33	N–C stretch
2.0 (±0.2)		0.0		1214	1219	1215	36	N–C stretch
5.3 (±0.4)		0.1		1273	1275 (1268)	1275	40	CH <sub>2</sub> twist + N–N stretch
				1387	1389 (1388)		44	CH <sub>2</sub> wag
				1433	1434 (1436)		46	CH <sub>2</sub> scissors
				1570	1573 (1576)		50	O–N–O stretch (eq)
				1593	1598 (1592)		51	O–N–O stretch (ax)
3.8 (±0.2)		0.1		2911			52	C–H stretch (ax)
4.0 (±0.3)		0.1		2949	2948		53	C–H stretch (ax)
3.2 (±0.3)		0.0		3001	3001 (3001)		56	C–H stretch (eq)
4.0 (±0.3)		0.0		3075	3075 (3074)		57	C–H stretch (eq)

<sup>a</sup> Previously reported vibrational frequencies collected at ambient conditions are summarized. Mode shifts (dν/dP)<sub>0</sub> are the linear slope of the frequencies with respect to pressure. The γ values are the least-squares fit to the Grüneisen equation.<sup>26</sup> <sup>b</sup> Frequency values were obtained from ref 17. <sup>c</sup> Frequency values in parentheses were obtained from ref 16. <sup>d</sup> Inelastic neutron scattering (INS) vibrational frequencies were obtained from ref 14.

observations. The 227 cm<sup>-1</sup> skeletal stretching feature splits into a doublet above 4.0 GPa with two clearly resolvable maxima at 249 and 285 cm<sup>-1</sup>. The new vibrational peaks at 386 and 419 cm<sup>-1</sup> become prominent features as the pressure is increased. Additionally, a large increase in the intensity of the 623 cm<sup>-1</sup> ring rocking vibration is observed in conjunction with a splitting of the mode. While the original characterization of γ-RDX eluded that the orthorhombic space group of α-RDX is retained,<sup>22</sup> it seems likely, on the basis of the changes in the vibrational pattern, that there is some pressure-induced deformation of the molecular structure of RDX associated with the γ → δ transition. However, a further description of the γ-RDX phase will require diffraction measurements with a complete refinement of the atomic positions.

The transition from the γ phase to the δ phase is associated with several noticeable changes in the spectroscopic pattern: (1) The Raman-active ring twisting doublet near 340 and 350 cm<sup>-1</sup> collapses into a single vibration. (2) The 890 cm<sup>-1</sup> ring breathing vibration shows a large frequency shift, and a new vibrational band develops on the high-frequency side. (3) Four clearly resolvable bands are observed in the C–H stretching region. (4) New Raman features are observed at 234, 431, and 987 cm<sup>-1</sup>. Vibrational modes with frequencies comparable to those at 234 and 431 cm<sup>-1</sup> have been noted in the Raman spectrum of β-RDX, suggesting similarities exist between the structures of the δ and β phases.<sup>18</sup> However, the vibrational pattern of the C–H stretching region is not consistent with that of β-RDX, providing strong evidence that phase is different. The infrared spectra above 17.8 GPa are of limited use in the characterization of the δ phase as the infrared spectral profiles

begin to broaden inhomogeneously, possibly due the sluggish phase transition.

The mode Grüneisen parameters, γ<sub>i</sub>, have been calculated for the Raman and infrared data of the α-RDX phase using the equations defined by Williams et al.<sup>26</sup> The equation of state obtained from Brillouin scattering (Hill average 11.99 GPa) was used to calculate the volume as a function of pressure.<sup>19</sup> We find an average unweighted Grüneisen parameter for all observed Raman modes of 0.2 and a corresponding value of 0.4 for the infrared modes. The larger infrared Grüneisen value can be understood to arise from the larger contribution of the two lowest frequency infrared active modes (105 and 150 cm<sup>-1</sup>) to the vibrational density of states.

## Conclusions

A systematic study of the changes in the vibrational spectra of RDX to 30 GPa has been presented. The Raman and IR vibrational patterns observed below 4.0 GPa are consistent with those previously defined for α-RDX. Our study finds evidence for two phases (γ and δ), and the kinetic stability of the γ phase has been extended to near 18 GPa. We suggest that the γ phase retains the crystallographic characteristics of the α phase, which is consistent with previous reports. We also suggest the α → γ transition is accompanied by pressure-induced molecular deformations, resulting in a lowering of the molecular symmetry. This is supported by the vibrational modifications accompanying this transition, such as the splitting of the vibrational modes, intensity changes, and large frequency shifts, but additional evidence must be provided by X-ray diffraction. New vibrational

features, which appear in the Raman spectrum near 18 GPa, as well as other spectroscopic changes, suggest a transition to a new phase ( $\delta$ ). As several of these new features occur at frequencies comparable to those observed in  $\beta$ -RDX, we suggest the two have a similar structure. Vibrational absorption spectra in the infrared provide information about the phase transitions which is consistent with that from the Raman data. X-ray diffraction studies in progress should elucidate the high-pressure structures of RDX.

**Acknowledgements.** We thank Dr. K. Clark of the Naval Surface Warfare Center based at Indian Head, MD, for providing the RDX samples. Far-IR measurements were performed at the U2A beamline at the NSLS of BNL (DOE Contract No. DE-AC02-98CH10886). The U2A beamline is supported by COMPRES, the Consortium for Materials Properties Research in Earth Sciences, under NSF Cooperative Agreement Grant No. EAR01-35554 and the U.S. DOE (CDAC, Contract No. DE-FC03-03N00144). A portion of this work was performed while J.A.C. held a National Research Council Resident Research Associateship Award at the U.S. Army Research Laboratory.

### References and Notes

- (1) Hultgreen, R. *J. Chem. Phys.* **1936**, *4*, 84.
- (2) McCrone, W. C. *Anal. Chem.* **1950**, *22*, 954.
- (3) Harris, P. M.; Reed, P. T. AFOSR-TR-59-165; Ohio State University Research Foundation: Columbus, OH, 1959.
- (4) Choi, C. S.; Prince, E. *Acta. Crystallogr.* **1972**, *B28*, 2857.
- (5) Kuklja, M. M.; Kunz, A. B. *J. Phys. Chem. Solids* **2000**, *61*, 35.
- (6) Kuklja, M. M.; Kunz, A. B. *J. Appl. Phys.* **2000**, *87*, 2216.
- (7) Kuklja, M. M.; Adeuv, B. P.; Aluker, E. D.; Krashennin, V. I.; Krechetov, A. G.; Mitrofanov, A. Y. *J. Appl. Phys.* **2001**, *89*, 4156.
- (8) Kunz, A. B. *Phys. Rev. B* **1996**, *53*, 9733.
- (9) Kuklja, M. M.; Stefanovich, E. V.; Kunz, A. B. *J. Chem. Phys.* **2000**, *112*, 3417.
- (10) Rogers, J. T. *Physical and Chemical Properties of RDX and HMX*; 20-P-26, Series B; Holston Defense Corp: Kingsport, TN, August 1962.
- (11) Sorescu, D. C.; Rice, B. M.; Thompson, D. L. *J. Phys. B* **1997**, *101*, 798.
- (12) Yoh, J. J.; McClelland, M. A.; Wardell, J. F.; Tarver, C. M. UCRL-JRNL-207203; Lawrence Livermore National Laboratory: Livermore, CA, 2004.
- (13) Cady, H. H. *J. Chem. Eng. Data* **1972**, *17*, 369.
- (14) Ciezak, J. A.; Trevino, S. F. *J. Phys. Chem. A* **2006**, *110*, 3759.
- (15) Haycraft, J. J.; Stevens, L. L.; Eckhardt, C. J. *J. Appl. Phys.*, in press.
- (16) Karpowicz, R. J.; Brill, T. B. *J. Phys. Chem.* **1984**, *88*, 348.
- (17) Rey-Lafon, M.; Trinquet-Coste, C.; Cavagnat, R.; Forel, M. T. *J. Chim. Phys.-Chim. Biol.* **1971**, *68*, 1533.
- (18) Torres, P.; Mercado, L.; Cotte, I.; Hernandez, S. P.; Mina, N.; Santana, A.; Chamberlain, R. T.; Lareau, R.; Castro, M. E. *J. Phys. Chem. B* **2004**, *108*, 8799.
- (19) Haycraft, J. J.; Stevens, L. L.; Eckhardt, C. J. *J. Chem. Phys.* **2006**, *124*, 024712.
- (20) See, for example: (a) Yoon, J. M.; Van, Aken, B.; Schnoor, J. L. *Int. J. Photoremediation* **2006**, *8*, 81. (b) Zhang, B.; Freitag, C. M.; Canas, J. E.; Cheng, Q.; Anderson, T. A. *Environ. Pollut.*, in press. (c) Smith, J. N.; Pan, X.; Gentles, A.; Smith, E. E.; Cox, S. B.; Cobb, G. P. *Environ. Toxicol. Chem.* **2006**, *25*, 446.
- (21) Nicol, M.; Oxley, J. C.; Baer, B. J. *High Pressure Res.* **1990**, *4*, 505.
- (22) Olinger, B.; Roof, B.; Cady, H. Los Alamos Scientific Laboratory Report LA-UR-78-1424; Los Alamos Scientific Laboratory: Los Alamos, NM, 1978.
- (23) Mao, H. K.; Xu, J.; Bell, P. M. *J. Geophys. Res.* **1986**, *91*, 4673.
- (24) Jayaraman, A. *Rev. Mod. Phys.* **1983**, *55*, 65.
- (25) Liu, Z.; Yang, H.; Hu, J.; Mao, H. K.; Hemley, R. J. *J. Phys.: Condens. Matter* **2002**, *14*, 10641.
- (26) Williams, Q.; Jeanloz, R.; Akaogi, M. *Phys. Chem. Miner.* **1986**, *13*, 141.